Ceramics International xxx (xxxx) xxx

Contents lists available at ScienceDirect

Ceramics International

journal homepage: www.elsevier.com/locate/ceramint

Work function and electrochemistry of ZnO (wurtzite) single crystals (F-1: L07)

Michael Vorochta [a], Vera Mansfeldova [b], Samiran Chakraborty [a], Ladislav Kavan [b,*]

[a] Department of Surface and Plasma Science, Faculty of Mathematics and Physics, Charles University, 180 00, Prague, 8, Czech Republic
[b] J. Heyrovský Institute of Physical Chemistry, Czech Acad. Sci., Dolejškova 2155/3, 182 00, Prague, 8, Czech Republic

ARTICLE INFO

Handling Editor: Dr P. Vincenzini

Keywords:
Interfaces (B)
Spectroscopy (B)
Surfaces (B)
ZnO (D)
Electrodes (E)

ABSTRACT

The work functions of two polar surfaces of ZnO (wurtzite), i.e., O-(000–1) and Zn-(0001) are determined by photoelectron spectroscopy in ultrahigh vacuum or in the presence of oxygen or water vapor at near-ambient pressures, and by Kelvin probe in air. The work functions were also determined by Mott-Schottky analysis in aqueous or aprotic (acetonitrile) electrolyte solutions. The values obtained by different techniques and in different environments are much less scattered compared to the fluctuations, reported for TiO_2 (anatase or rutile). The Zn-(0001) surface has a smaller work function for all the solid/vacuum and solid/gas interfaces, and also in the acetonitrile electrolyte solution. Solely at the aqueous electrochemical interface, the difference is small or even opposite. We propose a hypothesis that the dissociative water adsorption on the O-(000–1) is responsible for this irregular downshift of the work function in aqueous medium.

1. Introduction

Zinc oxide is a direct band-gap (≈3.1–3.4 eV) n-type semiconductor with high mobility (hundreds of $cm^2\ V^{-1}s^{-1}$), predetermining it for applications in energy conversion & storage, photo/catalysis, opto-electronics, sensors, spintronics etc. [1]. The energy-related applications include solar cells (both dye-sensitized [2,3] and perovskite [4,5]), Li-ion batteries [6], and production of hydrogen, being a prospective energy vector for the 21st century. Hydrogen can be generated on ZnO either by photoelectrochemical water splitting (Eq. (1a)) [7–9], or by dark catalysis of the CO_2-selective steam reforming of methanol (Eq. (1b)) [10]:

$$H_2O \rightarrow H_2 + ½\ O_2 \quad (1a)$$

$$CH_3OH + H_2O \rightarrow CO_2 + H_2 \quad (1b)$$

The photoelectrochemical water splitting (Eq. (1a)) occurs on ZnO with nearly 100 % faradaic efficiency, and with external quantum efficiency (IPCE) exceeding 90 % [11]. Yet, the optimization of n-ZnO for a practical photo/electrode material or catalyst includes, *inter alia,* mapping of its electronic structure near the conduction band minimum (CBM). A basic parameter, characterizing the electronic structure, is the work function, φ (which is numerically equivalent to the energy of Fermi level, E_F) [12,13]. It is also related to the energy of conduction band minimum (E_{CBM}):

$$\varphi = -E_F = -E_{CBM} + \frac{k_B T}{e} ln\left(\frac{N_C}{N_D}\right)\ ;\ N_C = 2\left(\frac{2\pi m^* k_B T}{h^2}\right)^{3/2} \quad (2)$$

k_B is the Boltzmann constant, T is temperature, e is the electron charge, N_C is the effective total concentration of conduction-band states at CBM, N_D is the concentration of ionized donors, m^* is the reduced mass of the electron, and h is the Planck constant.

The common experimental methods to determine φ, E_{CBM} and N_D are: photoelectron spectroscopy (UPS, XPS), Kelvin probe, and electrochemical impedance spectroscopy (EIS), the latter providing N_D and the flatband potential (V_{fb}) from the Mott-Schottky analysis [14–17]. Recently, Kawano [12] compiled work functions of elements, noticing strong fluctuations depending on the method, specimen, researcher, etc., but values from photoelectron spectroscopy usually tend to be smaller than values from Kelvin probe [12].

The work function controls the energy-level alignment at the oxide/oxide [18] or oxide/molecule [19] interfaces. Yet, the strong dependence of φ on experimental conditions, which may or may not be under control [12–17,20–25], is a challenge. This, on the other hand, allows for wide tuning of φ and E_{CBM} for applications in photovoltaics, catalysis, Li-batteries and solar fuel generation. The easiest way of φ tuning

* Corresponding author.
E-mail address: kavan@jh-inst.cas.cz (L. Kavan).

https://doi.org/10.1016/j.ceramint.2024.11.066
Received 13 September 2024; Received in revised form 2 November 2024; Accepted 5 November 2024
Available online 6 November 2024

consists in the removal of oxygen atoms from the ZnO surface by, e.g., a heat treatment. Thus formed oxygen vacancies, acting as n-dopants, raise the Fermi level, i.e., decrease the work function (Eq. (2)); the extra oxygen interstitials act oppositely [19,24]. Various metal oxides exhibit a correlation between their work function and the oxidation state of the metal [24]. Besides oxygen vacancy/interstitials, also doping of ZnO with heteroatoms has been used for fine-tuning of its work function [26–28]. Yet another approach of φ tuning consists in adsorption of suitable organic molecules; for instance, various derivatives of phosphonic acid enabled the φ tuning over a range of more than 1.5 eV (with a good correlation with the dipole moment of the adsorbate) [29].

Zinc oxide crystals possess hexagonal wurtzite structure ($P6_3mc$) exposing typically the polar C-faces (0001) and (000–1), which are Zn-terminated and O-terminated, respectively (Fig. 1). The polar faces are surprisingly stable [30,31], which is, reportedly, not observed in any other oxide [32]. Fig. 1 demonstrates that this unique structure induces an electric field in the direction from the Zn-(0001) to the O-(000–1) surfaces. The field boosts the X-ray photoelectron emission from the Zn-(0001) surface [33,34]. Furthermore, the electric field promotes photoelectrochemical water splitting (Eq (1a)) on the O-(000–1) surface by pushing the photogenerated holes towards the interface [11]. Interestingly, another abundant face on ZnO (wurtzite), i.e., (10-10), also called M-plane (cf. Fig. 1), is unstable at moderate pressures of water (≈1 mbar), and converts to terraces with the O-(000–1) and Zn-(0001) steps [35]. Obviously, the inter-relation of photoelectron spectroscopy and (photo)electrochemistry on ZnO provides a powerful tool for the investigation of built-in electric field in the bulk crystal and at the electrochemical interface (band bending).

The Zn-(0001) surface shows a fully occupied (1 x 1) overlayer of oxygen atoms or surface hydroxyls sitting at the Zn-terminating atoms [36]. The O-(000–1) face is characterized by an ordered (1 x 3) oxygen vacancy structure, which simply converts to the (1 x 1) OH-terminated surface by dissociative water adsorption [37]. This face is prone to reversible cycling of the work function simply by heat treatment, by dosing of H_2O/H_2, and by atmospheric exposure; while even the semiconductor-to-metal transition has been observed at an H-coverage of about 0.9 monolayers [38]. In contrast, the Zn-terminated face, Zn-(0001), is significantly more robust against the φ-tuning. For instance, the depleted Zn-(0001) surface cannot be prepared by sole heat treatment [38].

In addition to the effects of surface reconstruction by heat treatment in ultrahigh vacuum (UHV), and by the adsorption of airborne humidity or oxygen, the electrochemical interface (investigated by Mott-Schottky analysis) introduces specific effects, which are associated with the electrochemical double-layer. For instance, the flatband potentials of polycrystalline ZnO thin films were almost pH-independent, in a striking difference from the behavior of other oxide semiconductors, e.g., TiO_2 and SnO_2, and even from the single-crystal ZnO, which all exhibit roughly the Nernstian pH-shift of the flatband potential (−59 mV/pH) [17].

Model studies of TiO_2 single crystal electrodes revealed that, for fundamental reasons, work function measured by EIS, photoelectron spectroscopy (UPS, XPS) or Kelvin probe can vary over a wide range of nearly 1 eV [23]. This finding is corroborated by density functional theory (DFT) calculations for adsorption of molecular and dissociated water [39,40]. They elucidated the environment-borne variations of the work functions in anatase/rutile TiO_2 [40]. We are currently unable to support our observations on ZnO (wurtzite) with a similar DFT-simulation, because the system is too complicated. Deak et al. [40,41] elucidated that the dissociative adsorption of water at TiO_2 anatase (101) is responsible for the flipping of CBM positions in anatase/rutile TiO_2 in aqueous vs. aprotic electrolyte solutions [23]. Hence, it is tempting to discuss the dissociative water adsorption on O(000–1) [37] in the same way.

Here we investigate the two prominent ZnO (wurtzite) surfaces, viz O-(000–1) and Zn-(0001) at well-defined conditions using various modes of photoelectron spectroscopy (UPS, XPS, NAP-XPS) and electrochemical impedance spectroscopy (Mott-Schottky analysis). Surprisingly enough, and to the best of our knowledge, the face-selective Mott-Schottky analysis of ZnO in aqueous electrolyte solution has been so far reported in just one work employing, moreover, a simple measurement at single-frequency only [11]. This obviously requires a deeper study, which is presented here. Our general motivation was collecting reliable experimental work functions by independent techniques and in various environments, which will enable subsequent fundamental analysis of this fascinating material.

2. Experimental section

2.1. Materials and electrodes

The ZnO single crystals (5 x 5 × 0.5 mm^3; wurtzite (0001)/(000–1) orientation) were from SurfaceNet, GmbH (Germany). No deliberate doping by chemical reduction was carried out, but the natural doping manifested itself by the yellow color of the crystals. To enhance the reproducibility of experiments, every crystal was initially analyzed using the gentlest technique, i.e. by the Kelvin probe (KP) measurement in air employing the same procedure as in our previous work [20]. The corresponding work functions (φ_K) were nearly identical to those reported in the cited work [20]; hence we skip here a detailed description and repeated studies. (In certain cases, we reproduced the KP measurement at the end of testing sequence, as detailed in Section 3.1). Photoelectron spectroscopy was usually the second experimental technique used, and the sequence of measurements was finalized by

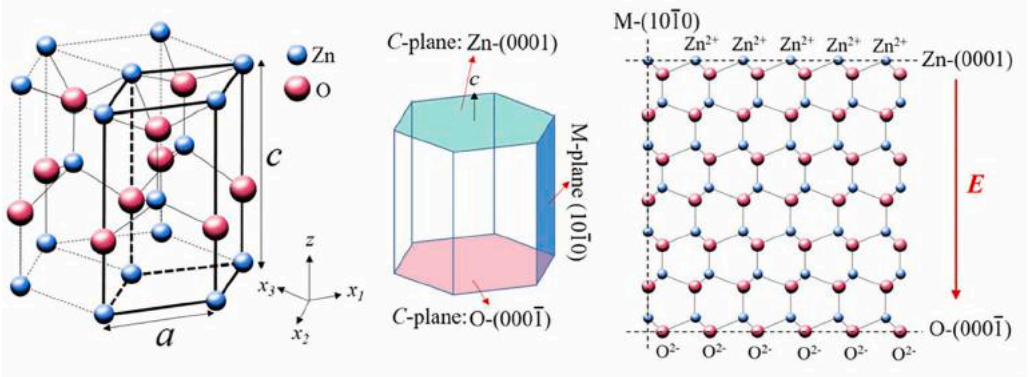

Fig. 1. The crystal structure of wurtzite ZnO and the schematic diagram to illustrate the exposed crystal facets. The vertical red arrow in the right chart shows the direction of the internal electrostatic field in ZnO. Reprinted with permission from Zhang et al. *Chem.Mater.* **28**, 6613 (2016) [11]. Copyright American Chemical Society. (For interpretation of the references to color in this figure legend, the reader is referred to the Web version of this article.)

electrochemistry. For electrochemical studies, we developed here an innovative mounting protocol, in which the Au-back-coated crystal was not epoxy-sealed as in Ref. [11], but positioned over an Au-sheet, and assembled by the laminating foils (Hewlett-Packard) by gentle hot-pressing. Fig. 2 shows the look of our mounted electrode. Our technique is obviously cleaner, because it avoids the problematic sealing of crystals, which is known to leave surface impurities from the uncured epoxy. Another advantage is the easy dismantling of the electrode, and good sealing tightness, which was satisfactorily resistant in both aqueous and acetonitrile electrolyte solutions.

2.2. Photoelectron spectroscopy

Photoelectron spectra were measured using a lab-based near-ambient X-ray photoelectron spectroscopy (NAP-XPS) system (SPECS Surface Nano Analysis, GmbH Germany) equipped with a high-pressure cell (DeviSIM NAP), the Al Kα X-ray source (XR-MF) and the differential pumping hemispherical electron energy analyzer (Phoibos 150 NAP 1D-DLD) designed for the high-pressure photoelectron measurements. The spectrometer allowed XPS analysis in a gas pressure range from $2\bullet10^{-9}$ up to 1 mbar. The high-resolution XPS spectra were recorded at 20 eV pass energy, while the 1 eV pass energy was used to measure the secondary electron cut-offs (SECO). To enhance the detection sensitivity of the secondary electron cut-off spectra, they were recorded under a negative sample bias of −15 V. This bias was subtracted from the kinetic energy of the photoelectrons during spectral processing, making the work function equal to the onset energy of the secondary electron intensity. In some cases, the kinetic energy of the photoelectrons was further corrected for surface charging effects, using the Zn $2p_{3/2}$ peak at 1022 eV as a reference. Further instrumental details are described elsewhere [42]. For a general description of the work function measurement, see Refs. [13,19]. The radio frequency (RF) plasma cleaner (Evactron E25), used for cleaning the ZnO surface, was operated at an RF frequency of 13.6 MHz with a power setting of 14 W in an oxygen atmosphere of 0.6 mbar (Linde, purity 5.0). The treatment duration was 5 min.

2.3. Electrochemical methods

Electrochemical impedance spectroscopy (EIS) was studied in a frequency range from 10 kHz to 1 Hz (modulation amplitude 10 mV) at varying potentials using an Autolab 302N potentiostat (Metrohm) equipped with a frequency response analyzer, and controlled by Nova 2.1 software. The counter-electrode was a Pt mesh. Studies in aqueous electrolyte solution employed an Ag/AgCl (3M KCl) reference electrode. The electrolyte solution was 0.5 M KCl saturated with ZnO; its pH was 6.5 (adjusted by diluted solutions of HCl or KOH). The potentials were recalculated, quoting the reversible hydrogen electrode (RHE) as the common reference [43]. The Nernstian pH-dependence (−59 mV/pH) is assumed for the calculation of the RHE potential [17,43]. Electrochemical measurements in an aprotic medium employed a non-aqueous Ag/AgCl reference electrode (sat. LiCl in ethanol) which was interfaced by a bridge with 0.1 M lithium bis(trifluoromethanesulfonyl)imide (LiTFSI) in acetonitrile. Its potential was regularly calibrated using ferrocene. For recalculation, the Fc^{+}/Fc redox potential was adjusted to 0.624 V vs. SHE [44]. All electrochemical measurements were made in a closed cell under an Ar atmosphere.

EIS spectra were fitted using the Zview (Scribner) software to a Randles-type circuit, in which R_{CT} (the charge-transfer resistance) is parallel to the constant phase element (*CPE*) [23,45–47]. The impedance of *CPE* equals [14,22,23]:

$$Z_{\mathrm{CPE}} = B^{-1}(i\omega)^{-\beta} \tag{3}$$

with ω being the EIS circular frequency, B (admittance pre-factor) and β (exponent) the frequency-independent parameters of the CPE ($0.8 \leq \beta \leq 1$). The interfacial capacitance, C is calculated from:

$$C = \frac{(R_{CT} \bullet B)^{1/\beta}}{R_{CT}} \tag{4}$$

Electrolytes, solvents, and other chemicals were of standard quality (p.a. or electrochemical grade) purchased from Aldrich or Merck. Acetonitrile was of the extra-dry quality, and further dried over a 4A molecular sieve (Aldrich). LiTFSI was dried under vacuum at 120 °C overnight. The water concentration in the final electrolyte solutions was between 10 and 20 ppm as analyzed by the Karl-Fischer titration (Mettler Toledo DL39 instrument).

3. Results and discussion

3.1. Photoelectron spectroscopy

As a first step (after the KP measurement, see Experimental Section) we performed a comprehensive XPS characterization of the as-received O-(000–1) and Zn-(0001) single crystal surfaces under ultra-high vacuum. Low-resolution survey spectra were initially measured within the binding energy range, capturing the main XPS lines of ZnO (see Fig. S1 of the ESI). Subsequently, a series of high-resolution spectra, including Zn 2p, O 1s, C 1s, and the valence band (VB), were acquired for each sample (Fig. 3). The survey spectra for both sample surfaces revealed solely the Zn- and O-related peaks, along with a minor C 1s signal attributed to

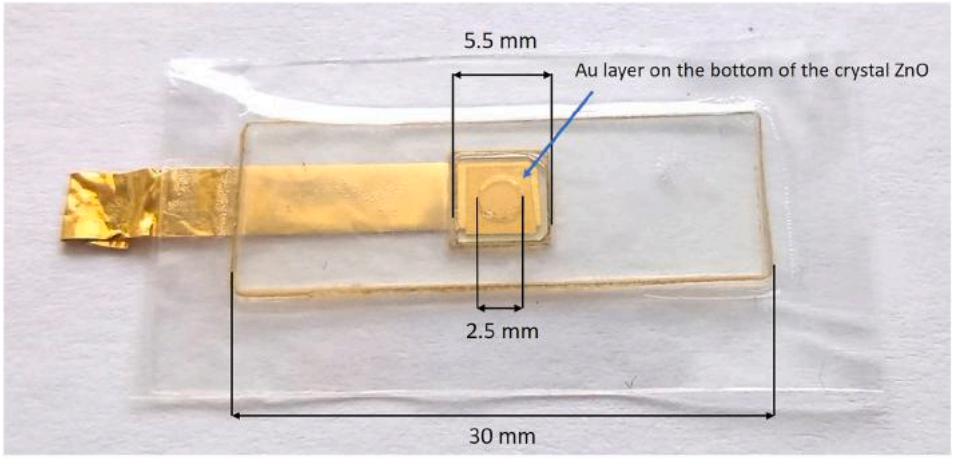

Fig. 2. The mounted ZnO crystal, 5 x 5 × 0.5 mm^3 assembled with Au-contacts by hot-pressed laminating foils. The top foil has a hole, 2.5 mm in diameter, to expose the crystal to the electrolyte solution. The crystal has an Au-layer on the back, which is mechanically pressed against the Au-foil.

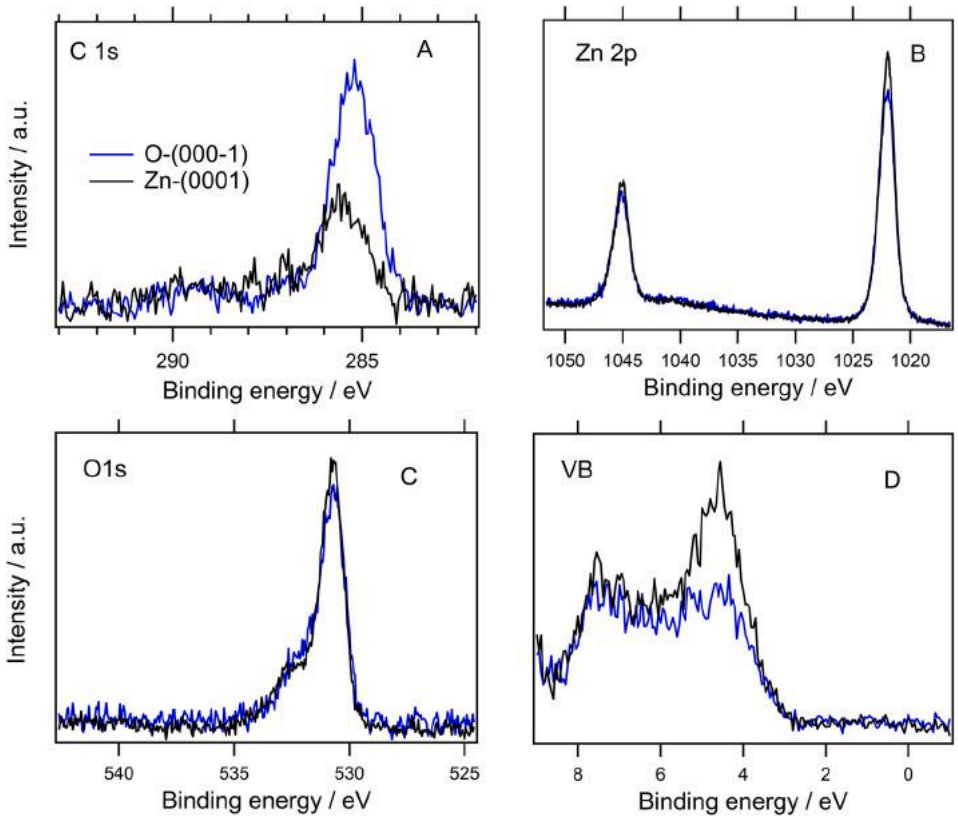

Fig. 3. Comparison of the C 1s (A), Zn 2p (B), O 1s (C) and valence band (VB) regions obtained from the as-received Zn- and O-terminated ZnO single crystals under UHV conditions. The spectra are displayed with absolute intensities (without normalization).

adventitious carbon.

Detailed C 1s spectra (Fig. 3A) indicated a significantly higher carbon presence on the O-(000–1) surface compared to the Zn-(0001) one. It is important to note that the C 1s peak for the O-(000–1) surface was initially detected at ca. 285.5 eV and was manually adjusted to 285.0 eV, which is the typical position for the C 1s peak of adventitious carbon on oxides [48,49]. In other words, the C 1s peak was used as a reference for the calibration of other XPS peaks affected by surface charging. For the Zn-(0001) sample, the calibration was performed using the position of its Zn 2p peak. All spectra were shifted by approximately 0.5 eV to lower binding energies, ensuring that the Zn 2p peak of the Zn-(0001) surface is aligned precisely with that of the O-(000-1) sample. This adjustment, however, led to a slightly higher C 1s peak position for the Zn-(0001) surface, which can be attributed to different interactions of carbon with the Zn-terminated surface.

The energy-calibrated Zn 2p spectra for both surfaces (Fig. 3B) consisted of a single doublet with peaks positioned at 1022–1045 eV, which are typical for Zn^{2+} ions in stoichiometric ZnO [49]. The only notable difference between the Zn 2p spectra of the two crystal faces was a slightly lower signal intensity for the O-(000–1) surface, likely due to signal attenuation from the higher level of surface contamination.

The corresponding O 1s spectra, shown in Fig. 3C, featured a dominant peak at approximately 530.6 eV, attributed to bulk oxygen in ZnO [33], and a broad shoulder at 532–533 eV, typically associated with various adsorbates from air, such as water, CO_x, OH, and other oxygen-containing species [50,51]. A detailed comparison of the spectra from different samples, however, revealed a similar trend to that observed in the Zn 2p spectra: attenuation of the ZnO-related signal and an increased signal from adsorbates in the case of the O-(000–1) surface.

The corresponding VB spectra (Fig. 3D) display characteristic shapes for Zn- and O-terminated ZnO surfaces, comprising three components located at 4.5 eV, 6.5 eV, and 7.5 eV [34,52]. According to the literature, the first component at 4.5 eV is associated with O 2p states and is more intense for the Zn-terminated ZnO surface. This increased intensity is typically attributed to a surface effect involving nonhybridized O-orbitals in OH groups present on the Zn-terminated surface [33].

Additionally, the valence band maximum (VBM) for both surfaces was observed at around 3 eV. Given that the band gap of ZnO is slightly above this value, the Fermi levels of both samples are likely positioned near the conduction band. This alignment suggests significant downward band bending and the formation of an electron accumulation layer on each surface in UHV.

XPS was employed to determine the surface work function (φ_X) of Zn- and O-terminated ZnO crystals. For these measurements, both samples were left ungrounded and biased at −15 V, which enabled the acquisition of their secondary electron cut-off edges using a hemispherical electron analyzer. This approach was used to calculate the φ_X values. A detailed procedure for determining φ_X using XPS is provided in Refs. [13,53]. Additionally, making XPS measurements under UHV conditions and in the presence of various gases allowed us to assess the impact of different gaseous atmospheres on the φ_X of the samples.

Fig. 4A shows the secondary electron (SECO) cut-offs of the Zn- and O-terminated ZnO single crystals measured under UHV conditions. The work functions, corresponding to the energy at the onset of the cut-offs, were determined to be about 3.9 eV and 4.1 eV for the Zn- and O-terminated surfaces, respectively (Table 1). These values were slightly lower than those measured using the Kelvin probe [20], prompting an investigation into the potential effects of oxygen and water on the surface work function. However, the work functions obtained by XPS under UHV conditions were almost identical to those measured using ultraviolet photoelectron spectroscopy (UPS) with a helium lamp operating in the He I mode, a more common technique for the work function measurement. Fig. S2A of the ESI presents the SECO cut-offs of the Zn-terminated sample obtained by XPS and UPS. The UPS spectrum

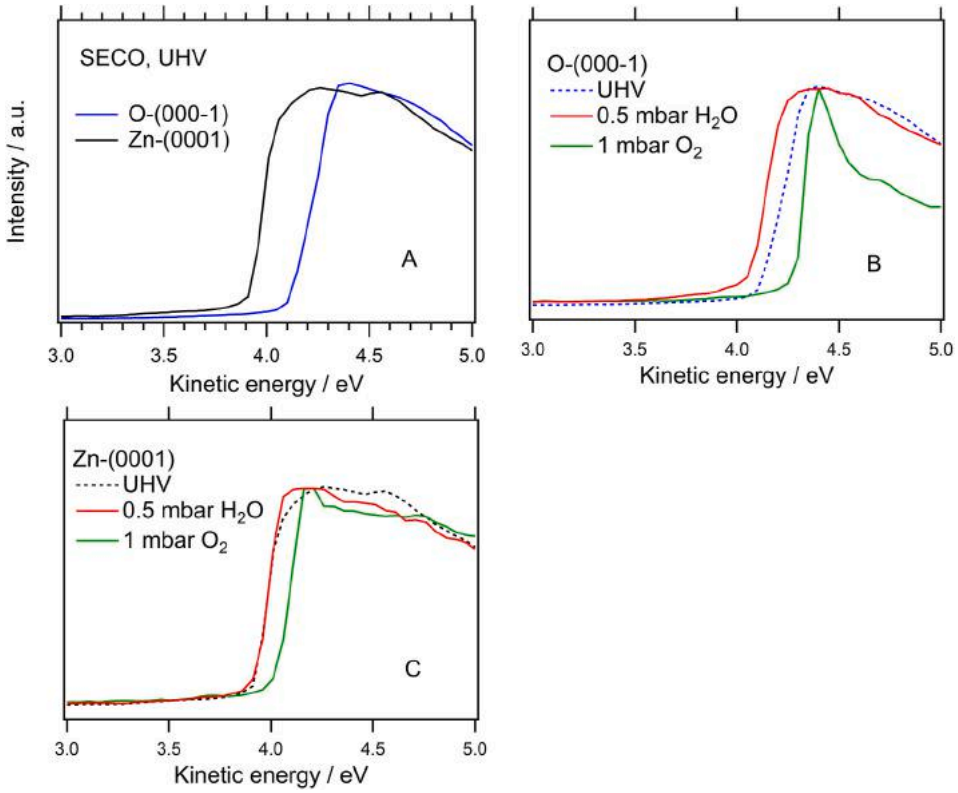

Fig. 4. Secondary electron cut-offs (SECO) measured by XPS from the as-received Zn- and O-terminated ZnO single crystals under UHV conditions (A). Charts (B) and (C) compare the secondary electron cut-off edges measured in UHV, O_2, and H_2O atmospheres on the O-terminated and Zn-terminated surfaces, respectively. The spectra have been normalized to have the same peak height.

shown in Fig. S2B, indicates that the VBM was observed at approximately 3 eV, consistent with the results obtained from XPS.

Fig. 4A and B illustrate the changes in SECO and in the corresponding φ_X values as a function of the atmosphere to which the crystals were exposed. Initially, the influence of 0.5 mbar of water was examined. The data show that water exposure decreased the φ_X of the O-terminated surface but had no noticeable effect on the Zn-terminated surface. Conversely, exposure to 1 mbar of O_2 affected both surfaces: the SECO of the O-terminated ZnO shifted by approximately 0.2 eV towards higher kinetic energy, raising the work function to about 4.3 eV. For the Zn-terminated sample, the SECO shifted by about 0.1 eV towards higher kinetic energies, resulting in a work function of approximately 4.0 eV.

In addition to the effects of water and oxygen atmospheres on ZnO crystals, we also investigated the influence of surface contaminants on the φ_X of the O-terminated ZnO surface. To achieve this, we tried to remove adsorbates from the as-received sample using O_2 RF plasma cleaning. The results of the cleaning process are shown in Figs. 5 and 6. They present XPS spectra acquired from the surface before and immediately after the O_2 RF plasma treatment, as well as from the cleaned surface after being relaxed in UHV for 24 hours. The plasma treatment significantly reduced surface contamination, resulting in an increased Zn 2p signal for the cleaned surface.

Additionally, there was a slight change in the O 1s spectrum at a binding energy of 532 eV (indicated by an arrow in Fig. 5), probably due to the partial removal of surface OH groups [38]. The SECO edge of this sample (Fig. 6) exhibits a pre-peak whose origin is unclear, but the extrapolated φ_X of the as-rec. sample is 4.1 eV (as in Fig. 4A and B). The plasma cleaning had a pronounced effect on φ_X, which increased by approximately 0.7 eV (see Fig. 6). However, after leaving the sample in UHV ($2 \bullet 10^{-9}$ mbar) for about 24 h, the φ_X decreased to around 4.3 eV. XPS analysis revealed that despite being in UHV, the sample surface was re-contaminated with carbon (the increased signal at 285 eV in Fig. 5B) and OH groups (the increased signal at 532 eV in Fig. 5C). Re-adsorption of impurities, even from UHV environment, was mentioned by others [29]. These measurements highlight that the conditions, under which the work function of ZnO is measured, significantly impact the obtained φ_X values.

The effect of impurities, if any, was also tested by Kelvin probe measurements on the virgin surfaces and the on same surfaces after passing all the tests (including electrochemistry, see below). The changes of φ_{KP} were generally small: 3.99 eV or 4.04 eV in the virgin or "used" Zn-(0001) surfaces, respectively, and 4.13 eV or 4.14 eV in the virgin/"used" O-(000–1) surfaces, respectively. Statistical analysis indicated the average deviation of the φ_{KP} to be ±0.030 eV. Hence, the measured φ_{KP} values are identical within experimental error, independent of the sample history. Though this finding enhances the information value of the KP measurements, the high sensitivity of φ_X to impurities, from the residual gases in UHV, appears to be specific to XPS only, most probably due to the slow adsorption kinetics of the impurities. Under ambient atmosphere, the surface converts to the "dirty" state immediately. Table 1 lists all measured work functions at different conditions.

3.2. Electrochemical impedance spectroscopy

Fig. 7 shows the Mott-Schottky plots of our ZnO crystal in aqueous and acetonitrile electrolyte solutions. The linear parts of the plots are fitted to the equation:

$$\frac{1}{C^2} = \left(\frac{2}{e\varepsilon_0\varepsilon_r N_D}\right)\left(V_{app} - V_{fb} - \frac{k_B T}{e}\right) + \frac{1}{C_H^2} \quad (5)$$

ε_0 is the permittivity of free space, ε_r is the dielectric constant (ε_r value for ZnO is 7.8 [8]), V_{app} is the applied potential. The Helmholtz capacitance, C_H, is the order of tens of $\mu F/cm^2$ [56,55], i.e. much larger than the space-charge capacitance, and consequently causing negligible contribution to Eq. (5). The second approximation consists in assuming

Table 1
Work functions for ZnO single crystal measured by various methods.

Method	Parameter [units]	(000–1) O-term	(0001) Zn-term	Ref.
UPS (in UHV)	φ_{UHVU} [eV]	–	3.8	This work
XPS (in UHV)	φ_{UHVX} [eV]	4.1	3.9	This work
NAP-XPS (0.5 mbar H_2O)	φ_X [eV]	4.0	3.9	This work
NAP-XPS (1 mbar O_2)	φ_X [eV]	4.3	4.1	This work
XPS (UHV, O_2 plasma)	φ_X [eV]	4.8	–	This work
Kelvin (in air)	φ_K [eV]	4.13	3.99	[20]
Kelvin (in air)	φ_K [eV]	4.13	3.99	This work
Kelvin (air; after all tests)	φ_K [eV]	4.14	4.04	This work
EIS-aqueous	V_{fb} [V_{RHE}]	0.20	0.23	[11]
EIS-aqueous	V_{fb} [V_{RHE}]	0.20	–	[54]
EIS-aqueous	V_{fb} [V_{RHE}]	0.17	0.20	This work
EIS-acetonitrile	V_{fb} [V_{Fc}]	−0.88	−0.96	[55]
EIS-acetonitrile	V_{fb} [V_{Fc}]	−0.87	−0.93	This work
EIS-aqueous	N_D [cm^{-3}]	$2.51\bullet10^{18}$	$4.79\bullet10^{17}$	[11]
EIS-aqueous	N_D [cm^{-3}]	$1.8\bullet10^{16}$	–	[54]
EIS-aqueous	N_D [cm^{-3}]	$6.9\bullet10^{17}$	$9.7\bullet10^{17}$	This work
EIS-acetonitrile	N_D [cm^{-3}]	$7.8\bullet10^{17}$	$1.5\bullet10^{18}$	[55]
EIS-acetonitrile	N_D [cm^{-3}]	$7.8\bullet10^{17}$	$8.5\bullet10^{17}$	This work
EIS-aqueous	φ_{fb} [eV]	4.11	4.14	[11,20]
EIS-aqueous	φ_{fb} [eV]	4.07	4.10	This work
EIS-acetonitrile	φ_{fb} [eV]	4.18	4.10	[55]
EIS-acetonitrile	φ_{fb} [eV]	4.18	4.08	This work

the projected electrode area for the calculation of capacitance (C). It is quite acceptable, considering our crystals are perfectly flat, exhibiting less than 1 % difference between the projected area and the AFM-measured "real" surface area [55].

Analysis of flatband potentials of oxide semiconductors in aqueous media is complicated by its pH dependence. It follows from the amphoteric surface groups (such as hydroxyls, which are de/protonated in alkaline/acidic solutions); furthermore, protons can be inserted into the oxide lattice in a way similar to the Li^+ insertion in aprotic media [17]. This dependence is material-specific, and never exactly Nernstian (−59 mV/pH) [17]. Secondly, the flatband potentials should be reported for pH corresponding to the isoelectric point of the oxide (IEP ≈8.8 for ZnO) [17,25]. The Fermi level position at zero band bending ($E_{F,fb}$) equals:

$$E_{F,fb} = -\varphi_{fb} = eV_0^{SHE} - eV_{fb}^{SHE,IEP} \quad (6)$$

Here, φ_{fb} is the work function derived from the flatband potential (also called "electrochemical work function") [20], V_0^{SHE} is the potential of the standard hydrogen electrode (SHE) in the absolute scale; $V_0^{SHE} \approx -4.44$ V [57]. The entry $V_{fb}^{SHE,IEP}$ is the flatband potential measured in the solution having pH equal to IEP, and referenced to SHE. Eq (6) can be rewritten into a more practical form:

$$\varphi_{fb} = 4.44 + V_{fb}^{RHE,pH} - 0.059\,pH - (IEP - pH) \bullet \chi \quad (7)$$

where "pH" is the actual pH of the used electrolyte solution (here 6.5) and χ is the average quasi-Nernstian pH-dependence of the flatband potential for the given oxide. The reported average values of χ are: −67

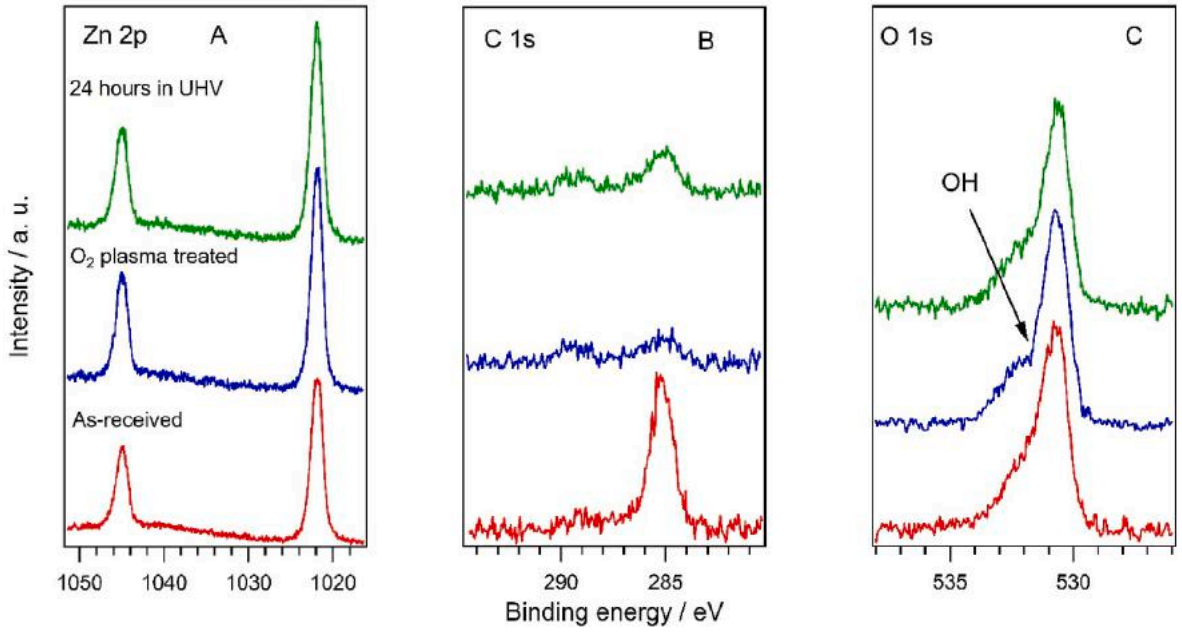

Fig. 5. Zn 2p (A), C 1s (B), and O 1s (C) UHV-XPS spectra were measured from the O-(000–1) surface of ZnO single crystal, which was treated by cleaning in O_2 plasma.

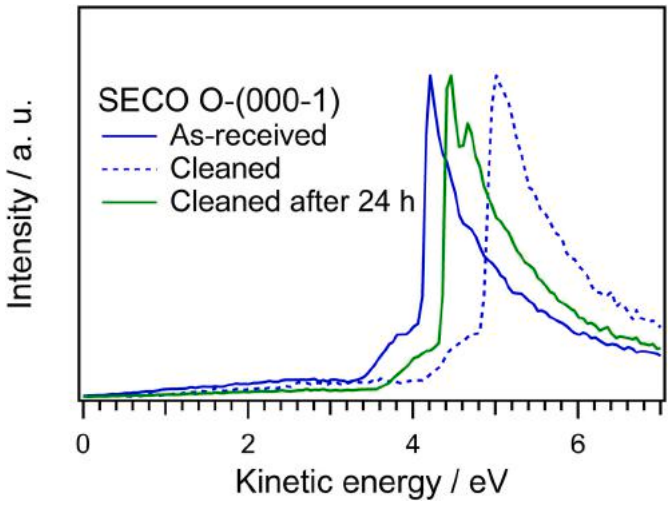

Fig. 6. Secondary electron cut-off measured by UHV-XPS on the as-received O-(000–1) surface of ZnO single crystal (blue curve), and that treated by cleaning in O_2 RF plasma. The blue dashed curve is for the sample measured immediately after the plasmatic cleaning. The green curve is for the same surface after 24 h storage in UHV. The spectra have been normalized to have the same peak height. (For interpretation of the references to color in this figure legend, the reader is referred to the Web version of this article.)

mV (ZnO single crystal), −4.8 mV (polycrystalline ZnO thin film), −50 mV (SnO_2 single crystal), and −60 mV (TiO_2 all morphologies) [17]. The pH-related complications are, obviously, absent in aprotic media, though a carefully dried electrolyte solution must be used (see Experimental Section), and the electrode potentials have to be normalized to a certain internal standard, such as ferrocene [20,23].

Table 1 lists the measured work functions together with other parameters obtained from the Mott-Schottky analysis (V_{fb} and N_D). Surprisingly, there are quite scarce data about the Mott-Schottky analysis of ZnO single-crystal electrodes [17]. The paper by Zhang et al. [11] appears to be the only work dealing with different V_{fb} values of the O-(000–1) and Zn-(0001) faces in an aqueous electrolyte solution. Another paper by Bohe et al. [54] reported solely the V_{fb} value for the O-(000–1) surface; yet their value agrees with that of Zhang et al. [11] (cf. Table 1). Considering the lack of reliable literature data, we revisited the problem once more again, and provided in Table 1 our own results for the O-(000–1) and Zn-(0001) surfaces.

The Mott-Schottky studies in aprotic media are scarce, too. To the best of our knowledge, there is only one paper dealing with the anisotropy of V_{fb} values of the O-(000–1) and Zn-(0001) faces in acetonitrile medium. The work function (φ_{fb}) was found to be smaller for the Zn-terminated face [55], which is exactly opposite to the stacking in aqueous medium [11]. This situation is reminiscent of the flipping of the φ_{fb} values for TiO_2 anatase and rutile single crystals in these two media [16,23]. Deak et al. [40,41] theoretically modelled the reversing of work functions by dissociative adsorption of water on the anatase surface. For ZnO (wurtzite), the Kelvin probe measurements [20] confirmed the same stacking of work function as in aprotic electrochemistry (Table 1). In other words, the O-/Zn-terminated faces of wurtzite qualitatively show *identical* response trends to aqueous/aprotic electrolyte solutions like anatase/rutile titania. Yet, the difference in φ_{fb} values, found in this, as well as in the earlier work [11], is quite small (≈3 meV, cf. Table 1). Even if we neglect the experimental errors of Mott-Schottky analysis, the sole inaccuracy of pH measurements (±0.05 pH) [22] would introduce the ±3 mV spread of the V_{fb} values, cf. Eq. (7). Hence, the flipping of work function of the O-(000–1) and Zn-(0001) faces at the ZnO (wurtzite) is unambiguously confirmed by neither study.

The Mott-Schottky analysis is known to overestimate the concentration of ionized donors, N_D [16,17,45], particularly in materials with a small effective electron mass ($m^* = 0.215 \bullet m_0$ for ZnO [58] m_0 is the electron mass at rest). The effective total density of states at the conduction band minimum (N_C see Eq. (2)) equals $2.5 \bullet 10^{18}$ cm^{-3} for ZnO ($2.94 \bullet 10^{18}$ cm^{-3} was reported in Ref. [34]). Hence, ZnO is assumed to be degenerate for N_D exceeding this limit. This does not occur for our crystals. Even for the largest N_D in Table 1, all our crystals behave like non-degenerate semiconductors. (Note that the mentioned extreme value comes from the literature [11]; and was obtained by a simple Mott-Schottky analysis at one single frequency only, and on a material, purchased from another producer). On the other hand, the N_D values for thin ZnO films are often much larger (of the order of 10^{20} cm^{-3}) [20,55]. They are very probably overestimated, which is elucidated by much smaller values found by, e.g., the Hall-effect [16,20]. We have no explanation for the striking difference between single crystals and thin-film specimens.

Fig. 8 shows an overview of all work function values measured by different techniques (cf. also Table 1). For comparison, our old data on TiO_2 single crystals, anatase (101) and rutile (001) [23] are shown too. Interestingly, the found values for ZnO (wurtzite) are much less scattered (fluctuating within a range of <0.4 eV) compared to >1 eV fluctuations of values for titania (anatase or rutile). The behavior of TiO_2 seems to be outstanding, even if we compare it with the (001) face of SnO_2 (cassiterite) [16]. Our systematically smaller work functions for the Zn-(0001) surface measured by photoelectron spectroscopy and

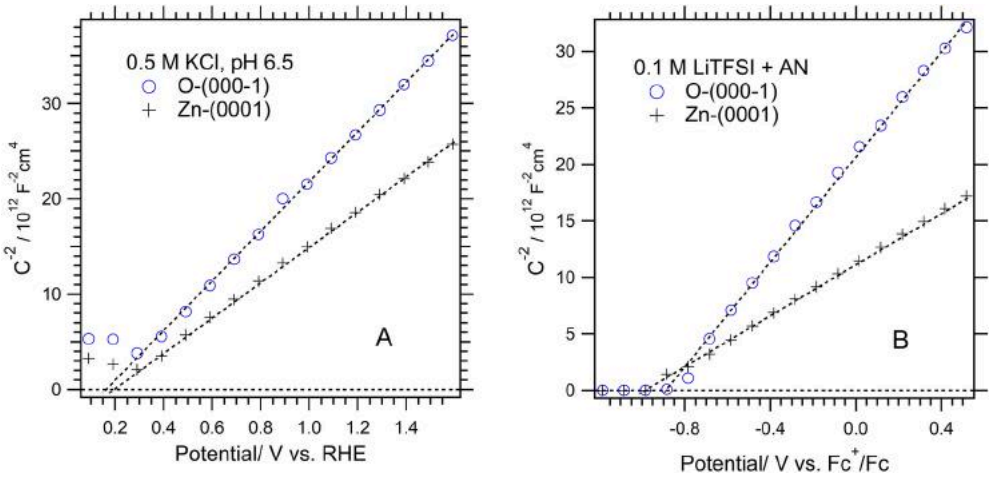

Fig. 7. Mott-Schottky plots for ZnO wurtzite single crystal electrodes in two orientations: O-terminated face, O-(000–1) and Zn-terminated face, Zn-(0001). The electrolyte solution is (A) 0.5 M aqueous KCl saturated with ZnO, pH 6.5 or (B) 0.1 M LiTFSI in acetonitrile.

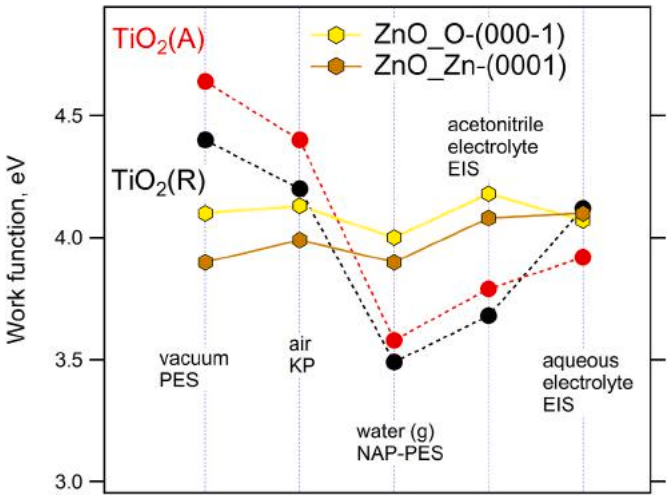

Fig. 8. Overview of work functions measured by various methods and environments on the ZnO (wurtzite) surfaces in orientations O-(000–1) and Zn-(0001), respectively. For comparison data for TiO_2 anatase (101) and rutile (001) from Ref. [23] are shown, too.

Kelvin probe are supported by earlier studies of polarity-dependent photoemission from ZnO (wurtzite) [33,34]. The stacking of Fermi levels is preserved in vacuum, air, oxygen and water vapor and even in the aprotic electrochemical interface, but it seems to flip specifically for the aqueous electrochemical interface. This mirrors exactly the situation in TiO_2 (anatase/rutile) [16,20,23]. The drop of "aqueous" φ_{fb} at anatase (101) was attributed to the dissociative adsorption of water at this surface [40,41]. The dissociative water adsorption was reported also for the O-(000–1) [37]. Though this would elegantly explain the same drop of "aqueous" φ_{fb} for our O-terminated wurtzite, this discussion would require a comparable-level DFT calculation of ZnO. This is a challenge for future efforts.

4. Conclusions

Systematic comparison of the work functions of two polar surfaces of ZnO (wurtzite), i.e., O-(000–1) and Zn-(0001) is based on photoelectron spectroscopy made either in ultrahigh vacuum or in the presence of oxygen and water vapor at near-ambient pressures. The work functions are also measured by the Kelvin probe in air.

The investigations of work functions at the ZnO/vacuum and ZnO/gas interfaces are upgraded by Mott-Schottky analysis from electrochemical impedance spectroscopy for both aqueous and aprotic (acetonitrile) electrolyte solutions.

The work functions of O-(000–1) and Zn-(0001) obtained by different techniques and in different environments are much less scattered (within a range of <0.4 eV) compared to the >1 eV fluctuations, which were previously found for TiO_2 (anatase or rutile). The Zn-(0001) surface has a smaller work function for all the solid/vacuum and solid/gas interfaces, and also for the electrochemical interface composed of aprotic (acetonitrile) electrolyte solution.

This uniform stacking of Fermi levels of Zn-(0001)/O-(000–1) surfaces seems to flip only at the aqueous electrochemical interface. Exactly the same occurs in TiO_2 (anatase/rutile), where the irregular drop of the "aqueous" φ_{fb} at anatase (101) was attributed to the dissociative adsorption of water, occurring selectively at this surface. The same mechanism, i.e., dissociative water adsorption on the O-(0001) could be responsible for the observed φ_{fb} shift at ZnO (wurtzite). However, theoretical analysis of this problem, at the level comparable to TiO_2, is still pending.

CRediT authorship contribution statement

Michael Vorochta: Writing – original draft, Validation, Project administration, Methodology, Investigation, Funding acquisition, Formal analysis, Data curation, Conceptualization. **Vera Mansfeldova:** Writing – review & editing, Writing – original draft, Investigation, Formal analysis, Data curation. **Samiran Chakraborty:** Investigation, Data curation. **Ladislav Kavan:** Writing – review & editing, Writing – original draft, Validation, Supervision, Resources, Project administration, Methodology, Investigation, Funding acquisition, Formal analysis, Data curation, Conceptualization.

Declaration of competing interest

The authors declare that they have no known competing financial interests or personal relationships that could have appeared to influence the work reported in this paper.

Acknowledgments

This work was supported by the Grant Agency of the Czech Republic (contract No. 22-24138S). The authors acknowledge the assistance provided by the Research Infrastructure NanoEnviCz, supported by MEYS CR under Project No. LM2023066 and project Pro-NanoEnviCz (Reg. No. CZ.02.1.01/0.0/0.0/16_013/0001821) supported by MEYS CR and EU - European Structural and Investments Funds. SC and MV acknowledge the Research Infrastructure SPL-HTC, supported by MEYS CR under Project No. LM2023072.

Appendix A. Supplementary data

Supplementary data to this article can be found online at https://doi.org/10.1016/j.ceramint.2024.11.066.

References

[1] M.A. Borysiewicz, ZnO as a functional material, a review, Crystals 9 (2019) 505.
[2] J.A. Anta, F. Guillet, R. Tena-Zaera, ZnO-Based dye-sensitized solar cells, J. Phys. Chem. C 116 (2012) 11413–11425.
[3] L. Kavan, Electrochemistry and dye-sensitized solar cells, Curr. Opin. Electrochem. 2 (2017) 88–96.
[4] P. Zhang, J. Wu, T. Zhang, Y. Wang, D. Liu, H. Chen, L. Ji, C. Liu, W. Ahmad, Z. D. Chen, S. Li, Perovskite solar cells with ZnO electron-transporting materials, Adv. Mater. 30 (2018).
[5] L. Kavan, Electrochemistry and perovskite photovoltaics, Curr. Opin. Electrochem. 11 (2018) 122–129.
[6] L. Wang, G. Zhang, Q. Liu, H. Duan, Recent progress in Zn-based anodes for advanced lithium ion batteries, Mater. Chem. Front. 2 (2018) 1414–1435.
[7] D. Dworschak, C. Brunnhofer, M. Valtiner, Photocorrosion of ZnO single crystals during electrochemical water splitting, ACS Appl. Mater. Interfaces 12 (2020) 51530–51536.
[8] R. Dom, H.G. Kim, P.H. Borse, Efficient hydrogen generation over (100)-oriented ZnO nanostructured photoanodes under solar light, CrystEngComm 16 (2014) 2432–2439.
[9] Y. Zhao, Z. Niu, J. Zhao, L. Xue, X. Fu, J. Long, Recent advancements in photoelectrochemical water splitting for hydrogen production, Electrochem. Energy Rev. 6 (2023) 14.
[10] H. Lorenz, M. Friedrich, M. Armbruster, B. Klotzer, S. Penner, ZnO is a CO_2-selective steam reforming catalyst, J. Catal. 297 (2013) 151–154.
[11] B. Zhang, Z. Wang, B. Huang, X. Zhang, X. Qin, H. Li, Y. Dai, Y. Li, Anisotropic photoelectrochemical (PEC) performances ff ZnO single-crystalline photoanode: effect of internal electrostatic fields on the separation of photogenerated charge carriers during PEC water splitting, Chem. Mater. 28 (2016) 6613–6620.
[12] H. Kawano, Effective work functions of the elements, Prog. Surf. Sci. 97 (2022) 100583.
[13] J.W. Kim, A. Kim, Absolute work function measurement by using photoelectron spectroscopy, Curr. Appl. Phys. 31 (2021) 52–59.
[14] A. Hankin, F.E. Bedoya-Lora, J.C. Alexander, A. Regoutz, G.H. Kelsall, Flat band potential determination: avoiding the pitfalls, J. Mater. Chem. A 7 (2019) 26162–26176.
[15] K. Sivula, Mott–Schottky analysis of photoelectrodes: sanity checks are needed, ACS Energy Lett. 6 (2021) 2549–2551.
[16] L. Kavan, Electrochemistry and band structure of semiconductors (TiO_2, SnO_2, ZnO): avoiding pitfalls and textbook errors, J. Solid State Electrochem. 28 (2024) 829–845.

[17] M.Y. Patel, M.J. Mortelliti, J.L. Dempsey, A compendium and meta-analysis of flatband potentials for TiO_2, ZnO, and SnO_2 semiconductors in aqueous media, Chem. Phys. Rev. 3 (2022) 011303.
[18] D.O. Scanlon, C.W. Dunnill, J. Buckeridge, S.A. Shevlin, A.J. Logsdail, S. M. Woodley, C.R.A. Catlow, M.J. Powell, R.G. Palgrave, I.P. Parkin, G.W. Watson, T.W. Keal, P. Sherwood, A. Walsh, A.A. Sokol, Band alignment of rutile and anatase TiO_2, Nat. Mater. 12 (2013) 798–801.
[19] M.T. Greiner, M.G. Helander, W.M. Tang, Z.B. Wang, J. Qiu, Z.H. Lu, Universal energy-level alignment of molecules on metal oxides, Nat. Mater. 11 (2012) 76–81.
[20] H. Krysova, V. Mansfeldova, H. Tarabkova, A. Pisarikova, Z. Hubicka, L. Kavan, High-quality dense ZnO thin films: work function and photo/electrochemical properties, J. Solid State Electrochem. 28 (2024) 2531–2546.
[21] L. Kavan, M. Zlamalova, V. Mansfeldova, H. Krysova, H. Tarabkova, B. Pitna Laskova, Interplay of band energetics and photo/electro/chemical activity of SnO_2 thin films, Monatsh. Chem. 155 (2024) 325–331.
[22] M. Zlamalova, V. Mansfeldova, H. Tarabkova, H. Krysova, L. Kavan, Variable work function of semiconducting thin-film oxide electrodes: a case study of SnO_2 and TiO_2, J. Solid State Electrochem. 27 (2023) 1935–1943.
[23] V. Mansfeldova, M. Zlamalova, H. Tarabkova, P. Janda, M. Vorokhta, L. Piliai, L. Kavan, Work function of TiO_2 (anatase, rutile, and brookite) single crystals: effects of the environment, J. Phys. Chem. C 125 (2021) 1902–1912.
[24] M.T. Greiner, L. Chai, M.G. Helander, W.M. Tang, Z.H. Lu, Transition metal oxide work functions: the influence of cation oxidation state and oxygen vacancies, Adv. Funct. Mater. 22 (2012) 4557–4568.
[25] R. Beranek, Photoelectrochemical methods for the determination of the band edge positions in TiO_2-based nanomaterials, Adv. Phys. Chem (2011) 786759–78675920.
[26] A. Douloumis, N.R.E. Vrithias, N. Katsarakis, I.N. Remediakis, G. Kopidakis, Tuning the workfunction of ZnO through surface doping with Mn from first-principles simulations, Surf. Sci. 726 (2022) 122175.
[27] A.K. Saikumar, S. Sundaresh, S.D. Nehate, J. Phelps, R. Abdolvand, K.B. Sundaram, Work function estimation of gallium-doped zinc oxide using transparent gate electrode MOSFET, ECS Journal of Solid State Science and Technology 12 (2023) 033010.
[28] S. Kyu Kang, D. Yun Kang, J. Wan Park, K. Rock Son, T. Geun Kim, Work function-tunable ZnO/Ag/ZnO film as an effective hole injection electrode prepared via nickel doping for thermally activated delayed fluorescence-based flexible blue organic light-emitting diodes, Appl. Surf. Sci. 538 (2021) 148202.
[29] I. Lange, S. Reiter, M. Pätzel, A. Zykov, A. Nefedov, J. Hildebrandt, S. Hecht, S. Kowarik, C. Wöll, G. Heimel, D. Neher, Tuning the work function of polar zinc oxide surfaces using modified phosphonic acid self-assembled monolayers, Adv. Funct. Mater. 24 (2014) 7014–7024.
[30] O. Dulub, U. Diebold, G. Kresse, Novel stabilization mechanism on polar surfaces: ZnO(0001)-Zn, Phys. Rev. Lett. 90 (2003) 016102.
[31] G. Kresse, O. Dulub, U. Diebold, Competing stabilization mechanism for the polar ZnO(0001)-Zn surface, Phys. Rev. 68 (2003).
[32] D. Mora-Fonz, T. Lazauskas, M.R. Farrow, C.R.A. Catlow, S.M. Woodley, A. A. Sokol, Why are polar surfaces of ZnO stable? Chem. Mater. 29 (2017) 5306–5320.
[33] M.W. Allen, D.Y. Zemlyanov, G.I.N. Waterhouse, J.B. Metson, T.D. Veal, C. F. McConville, S.M. Durbin, Polarity effects in the x-ray photoemission of ZnO and other wurtzite semiconductors, Appl. Phys. Lett. 98 (2011).
[34] R. Heinhold, M.W. Allen, Polarity-dependent photoemission of in situ cleaved zinc oxide single crystals, J. Mater. Res. 27 (2012) 2214–2219.
[35] S. Wenzel, I.M.N. Groot, ZnO(101¯0) is unstable in moderate pressures of water, Surf. Sci. 715 (2022) 121940.
[36] C.M. Schleputz, Y. Yang, N.S. Husseini, R. Heinhold, H.S. Kim, M.W. Allen, S. M. Durbin, R. Clarke, The presence of a (1 x 1) oxygen overlayer on ZnO(0001) surfaces and at Schottky interfaces, J. Phys. Condens. Matter 24 (2012) 095007.
[37] M. Kunat, S.G. Girol, U. Burghaus, C. Woell, The interaction of water with the oxygen-terminated, polar surface of ZnO, J. Phys. Chem. B 107 (2003) 14350.
[38] R. Heinhold, G.T. Williams, S.P. Cooil, D.A. Evans, M.W. Allen, Influence of polarity and hydroxyl termination on the band bending at ZnO surfaces, Phys. Rev. 88 (2013).
[39] D.D. Nematov, K.T. Kholmurodov, M.A. Husenzoda, A. Lyubchyk, A. S. Burhonzoda, Molecular adsorption of H_2O on TiO_2 and TiO_2:Y surfaces, J. Human, Earth Future 3 (1922) 213–222.
[40] P. Deak, J. Kullgren, B. Aradi, T. Frauenheim, L. Kavan, Water splitting and the band edge positions of TiO_2, Electrochim. Acta 199 (2016) 27–34.
[41] J. Kullgren, B. Aradi, T. Frauenheim, L. Kavan, P. Deak, Resolving the controversy about the band alignment between rutile and anatase: the role of OH-/H+ adsorption, J. Phys. Chem. C 119 (2015) 21952–21958.
[42] M. Vorokhta, I. Khalakhan, M. Vondráček, D. Tomeček, M. Vorokhta, E. Marešová, J. Nováková, J. Vlček, P. Fitl, M. Novotný, P. Hozák, J. Lančok, M. Vrňata, I. Matolínová, V. Matolín, Investigation of gas sensing mechanism of SnO2 based chemiresistor using near ambient pressure XPS, Surf. Sci. 677 (2018) 284–290.
[43] G. Jerkiewicz, Standard and reversible hydrogen electrodes: theory, design, operation, and applications, ACS Catal. 10 (2020) 8409–8417.
[44] V.V. Pavlishchuk, A.W. Addison, Conversion constants for redox potentials measured versus different reference electrodes in acetonitrile solutions at 25°C, Inorg. Chim. Acta. 298 (2000) 97–102.
[45] L. Kavan, L. Steier, M. Grätzel, Ultrathin buffer layers of SnO_2 by atomic layer deposition: perfect blocking function and thermal stability, J. Phys. Chem. C 121 (2017) 342–350.
[46] L. Kavan, N. Tetreault, T. Moehl, M. Grätzel, Electrochemical characterization of TiO_2 blocking layers for dye sensitized solar cells, J. Phys. Chem. C 118 (2014) 16408–16418.
[47] T. Moehl, J. Suh, L. Severy, R. Wick-Joliat, S.D. Tilley, Investigation of (leaky) ALD TiO_2 protection layers for water-splitting photoelectrodes, ACS Appl. Mater. Interfaces 9 (2017) 43614–43622.
[48] M.C. Biesinger, Accessing the robustness of adventitious carbon for charge referencing (correction) purposes in XPS analysis: insights from a multi-user facility data review, Appl. Surf. Sci. 597 (2022).
[49] B.V. Crist, XPS in industry—problems with binding energies in journals and binding energy databases, J. Electron. Spectrosc. Relat. Phenom. 231 (2019) 75–87.
[50] R. Al-Gaashani, S. Radiman, A.R. Daud, N. Tabet, Y. Al-Douri, XPS and optical studies of different morphologies of ZnO nanostructures prepared by microwave methods, Ceram. Int. 39 (2013) 2283–2292.
[51] T.J. Frankcombe, Y. Liu, Interpretation of oxygen 1s X-ray photoelectron spectroscopy of ZnO, Chem. Mater. 35 (2023) 5468–5474.
[52] P.D.C. King, T.D. Veal, A. Schleife, J. Zúñiga-Pérez, B. Martel, P.H. Jefferson, F. Fuchs, V. Muñoz-Sanjosé, F. Bechstedt, C.F. McConville, Valence-band electronic structure of CdO, ZnO, and MgO from x-ray photoemission spectroscopy and quasi-particle-corrected density-functional theory calculations, Phys. Rev. 79 (2009).
[53] G. Shao, Work function and electron affinity of semiconductors: doping effect and complication due to Fermi level pinning, Energy & Environmental Materials 4 (2021) 273–276.
[54] A.E. Bohe, J.R. Vilche, K. Jüttner, W.J. Lorenz, W. Kautek, W. Paatasch, An electrochemical impedance spectroscopy study of passive zinc and low alloyed zinc electrodes in alkaline and neutral aqueous solutions, Corrosion Sci. 32 (1991) 621–633.
[55] L. Kavan, H. Krysova, M. Zukalova, H. Tarabkova, Z. Hubicka, Peculiar photoelectrochemical activity of zinc oxide and tin dioxide, J. Photochem. Photobiol., A, 458 (2025) 115929.
[56] A.C. Guler, J. Antos, M. Masar, M. Urbanek, M. Machovsky, I. Kuritka, Comprehensive evaluation of photoelectrochemical performance dependence on geometric features of ZnO nanorod electrodes, Nanoscale Adv. 5 (2023) 3091–3103.
[57] J. Bisquert, P. Cendula, L. Bertoluzzi, S. Gimenez, Energy diagram of semiconductor/electrolyte junctions, J. Phys. Chem. Lett. 5 (2014) 205–207.
[58] Z.H. Zhang, M. He, Q. Li, Obtaining the effective electron mass from valence electron energy-loss spectroscopy, Solid State Commun. 149 (2009) 1856–1859.